A preliminary assessment of olivine phenocrysts from the monogenetic basalt of the McCartys Flow, Zuni-Bandera Volcanic Field, New Mexico

Gary S. Michelfelder, Lawrence K. Horkley, Clayton Reinier, and Sarah Hudson
2021, pp. 141-152. https://doi.org/10.56577/FFC-71.141

in:

Geology of the Mount Taylor area, Frey, Bonnie A.; Kelley, Shari A.; Zeigler, Kate E.; McLemore, Virginia T.; Goff, Fraser; Ulmer-Scholle, Dana S., New Mexico Geological Society 71st Annual Fall Field Conference Guidebook, 310 p. https://doi.org/10.56577/FFC-71

This page is intentionally left blank to maintain order of facing pages.

New Mexico Geological Society Guidebook, 71st Field Conference, Geology of the Mount Taylor Area, 2021, p. 141-152.

A PRELIMINARY ASSESSMENT OF OLIVINE PHENOCRYSTS FROM THE MONOGENETIC BASALT OF THE MCCARTYS FLOW, ZUNI-BANDERA VOLCANIC FIELD, NEW MEXICO

Gary S. Michelfelder[1], Lawrence K. Horkley[2], Clayton Reinier[1], and Sarah Hudson[1]

[1]Department of Geography, Geology and Planning, Missouri State University, 901 S. National Ave., Springfield, Missouri 65897, USA
[2]Department of Earth and Environmental Sciences, University of Iowa, 115 Trowbridge Hall, Iowa City, Iowa, 52242, USA

Abstract—Monogenetic small-volume basaltic volcanoes are the most abundant subaerial volcanic landforms on Earth but are some of the most poorly understood systems. Their short durations, small volumes, and lack of recurrence make monitoring and hazard assessment difficult. The Zuni-Bandera volcanic field in western New Mexico contains small-volume basaltic centers erupting tholeiitic to alkalic basalts. Evidence shows no correlation of magma composition with eruption age, location, or volumetric output, prompting questions about the influence of magma ascent rates, magma storage conditions, and mantle source characteristics on lava compositions. Here, we present olivine major and minor element mineral chemistry from the 3200-year-old McCartys Flow, the youngest tholeiite basalt in the volcanic field. Olivine displays four phenocryst types with unique textures and major and minor element compositions. Multiple olivine types co-exist at the thin section scale. Major and minor element diffusion at frozen melt–phenocryst interfaces was modeled, revealing magma residence times ranging from 3–9 months. Type 3 olivine phenocrysts require step function initial conditions and record diffusion re-equilibration followed by magma mixing. These profiles indicate the magma resided in the reservoir for 10–15 years and accumulated from multiple batches of mixed magmas less than 10 days before the eruption. Our results show that primitive magmas in small-volume monogenetic volcanoes have complex lithospheric magmatic histories and stored in magma bodies influenced by an open system to develop different local chemical environments.

INTRODUCTION

Deciphering the petrologic processes leading to an eruption in small-volume monogenetic volcanic fields offers many petrologic and volcanological challenges. Monogenetic volcanoes are amongst the most abundant volcanic features on Earth. Still, since they erupt small volumes of chemically and petrographically "simple" magmas, they have been understudied by volcano petrologists compared to their polygenetic counterparts (McGee and Smith, 2016). The idea of "monogenetic" behavior is further complicated by different meanings of the term "monogenetic." Volcanologically, it is defined as temporally limited cone building (Nemeth and Kereszturi, 2015), while geochemically, the term defines a batch of magma generated by a single continuous process. These definitions have led to small-volume volcanoes that are the product of distinct magma batches described as volcanologically monogenetic, even though these systems are not geochemically monogenetic (Brenna et al., 2010).

Furthermore, the transition between small-volume monogenetic systems and medium to large polygenetic systems is poorly defined. The poorly defined transition has led to a model for small volume basaltic "monogenetic" magmatic systems where magma ascends to eruption rapidly (days to months) from the mantle or lower crustal source area after magma generation, with little to no magma storage in the upper crust (McGee et al., 2012; 2013). This idea has persisted even though a wide range in mineral compositions and textures are commonly preserved in the rock, suggesting open or partially open magmatic systems (McGee et al., 2011, 2012, 2013; McGee and Smith, 2016; Re et al., 2017; Coote et al., 2019). Over the past two decades, the study of zoned magmatic crystals has become an indispensable tool for resolving these processes and their timescales and suggest "monogenetic" magmas may range from simple melting of a homogenous source to more complicated melting of a multi-component source (Costa et al., 2008; McGee et al., 2011, 2012, 2013; McGee and Smith, 2016; Rubin et al., 2017; Costa et al., 2020). Detailed studies of volcanic sequences within small-volume monogenetic basaltic volcanic fields suggest the relationship of chemical composition to stratigraphic sequence is far from simple. The complex magmatic processes reflect those observed at polygenetic systems where diverse crystal populations reflect multi-level storage systems that extend through the entirety of the crust with a range of conditions for crystallization (McGee et al., 2012; Cashman et al., 2017; Johnson and Cashman, 2020).

In this study, we present a preliminary study of olivine phenocryst compositions, textures, and diffusion chronometry to characterize the magma storage conditions and transport leading up to the eruption of the McCartys Flow in the Zuni-Bandera volcanic field, New Mexico (Fig. 1). Olivine provides an opportunity to investigate deeper parts of the magmatic system and is more likely to yield information on the mantle source before crustal contamination or magma differentiation during magma migration to the surface. We infer four olivine crystal types based on texture and core-to-rim composition-

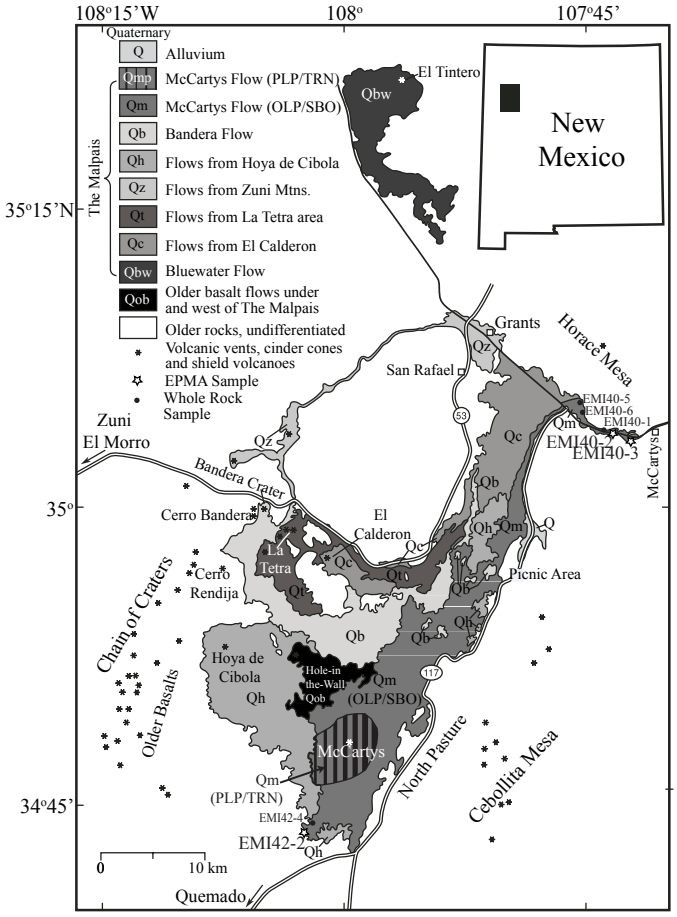

FIGURE 1. Location map of the Zuni-Bandera volcanic field showing the Bandera (Qb) and McCartys (Qm) flows and sample locations. Samples selected for olivine mineral chemistry are from the olivine-phyric basalt group and locations are shown by stars. Modified from Sims et al. (2007).

al transects. Three types have cognate origins, and the fourth outlier type has a non-cognate source and provides evidence for magma differentiation and evolution during ascent through the crust.

BACKGROUND

The Zuni-Bandera volcanic field (ZBVF) is in west-central New Mexico along the Arizona-New Mexico border (Fig. 1). Volcanic rocks comprise a sequence of mixed tholeiite and alkali basalt lava flows, spatter and scoria cones, small shield volcanoes, maars, and collapse pits (Baldridge et al., 1991; Menzies et al., 1991; Peters et al., 2008) erupted in the transitional zone between Rio Grande rift and Basin and Range extensional zones, and the relatively stable Colorado Plateau. The ZBVF is one of a series of NE-SW-aligned volcanic fields along the Jemez Lineament, which stretches from the Springer volcanic field in Arizona to the Clayton-Raton volcanic field along the New Mexico-Colorado border (Magnani et al., 2004). Geophysical studies of the Jemez Lineament suggest it may act as a conduit for melt transport away from the locus of active magmatism within the Rio Grande rift (Magnani et al., 2004; Deng et al., 2017).

Volcanism in the ZBVF occurred in three general pulses of activity in the last 700 ka (Laughlin et al., 1993; 1994; Sims et al., 2007). Two older pulses occurred at 700 ka and 150 ka. The third and youngest pulse began around 75 ka and includes the Bluewater (68 Ka), Paxton-Twin Craters (15 to 20 ka), Bandera (10 ka), and McCartys (3200 years) lavas (Laughlin et al., 1994; Dunbar and Phillips, 2004; Sims et al., 2007). The 3200 year-old McCartys Flow originates from the monogenic McCartys crater (Fig. 1) and is the youngest dated lava in the ZBVF (Laughlin et al., 1994). McCartys lava samples are vesicular, porphyritic basalts with plagioclase and euhedral to anhedral olivine phenocrysts, representing typical ZBVF tholeiitic basalt (Carden and Laughlin, 1974; Kolisnik, 1997). Plagioclase phenocrysts are subhedral to euhedral and strongly zoned with sieved cores. Augite clinopyroxene phenocrysts (>0.3 mm) when present, are skeletal, but euhedral microphenocrysts (<0.3 mm) are common. The groundmass is pilotaxitic trachytic, composed of laths of unzoned plagioclase, glass, and sparse to rare euhedral olivine and augite pyroxenes (Laughlin et al., 1972; Carden and Laughlin, 1974; Kolisnik, 1997). Consistent rare earth element (REE) patterns and Sr, Nd, and Pb isotope ratios from whole rock and olivine-hosted melt inclusions suggest the basalts are derived from variable crustal contamination of primary mafic materials sourced from partial melting of the mantle within the garnet facies (Levesque and Ramos, 2016, 2017).

Carden and Laughlin (1974) described textural and chemical variation along strike of the McCartys Flow. The modal volume and size of plagioclase was used to divide the flow into two basalt groups: olivine-phyric and plagioclase-phyric. Kolisnik (1997) further divided the McCartys basalt flow into four basalt groups: olivine-phyric (OLP), plagioclase-phyric (PLP), transitional (TRN), and subophitic (SBO) based on geochemical evidence. McCartys Flow basalts show a spatial distribution function of the relative position to the source scoria cone (Fig. 1). The four basalt groups show a concentric spatial distribution pattern around the central cinder cone near the southern end of the flow. Much of the flow length is homogeneous OLP basalt, but some variation occurs in the vicinity of the central cone. The OLP basalts are characterized by more fluid flow features as indicated by pahoehoe ropes, pressure ridges, and collapse depressions over lava tubes suggesting a rheological difference in the basalt types during movement. The SBO basalts are restricted to the northern distal part of the lava flow and are interfingered with the OLP lavas. They are difficult to distinguish in the field. This basalt group is either a textural subtype of the OLP basalts or a separate flow unit (Kolisnik, 1997).

Transitional (TRN) basalts are spatially between the OLP, PLP, and SBO with gradational contacts. Their presence likely suggests that phase relationships between basalt types are more complicated than those described by Carden and Laughlin (1974) or Kolisnik (1997). The concentric petrologic basalt facies suggests that the cinder cone is the eruptive center for the PLP and TRN basalts and potentially the OLP basalts. However, the OLP basalts could have erupted from fissures (Kolisnik, 1997). Plagioclase-phyric basalts are restricted to

within ~4 km of the cone. Smooth hexagonally jointed domes characterize PLP basalt morphology. Pressure ridges and acuate collapse structures are rare compared to the OLP basalt morphology.

METHODS

Six whole-rock samples of unweathered rock were collected from the OLP basalt group of the McCartys Flow. Two samples were collected from south of the McCartys crater, and four samples were collected from the distal northern extent of the flow north of and along Interstate 40. Standard thin sections of each sample were used to determine mineral percentages, size, and shape and to describe igneous textures and structures. Microprobe polished thin sections were made for three samples, two from north of the crater along Interstate 40 and one from south of the crater. No polished thin sections from the PLP, SBO, or TRN basalt groups are included in this study. Olivine mineral analyses were based on olivine phenocryst size distributions, vesicularity of the sample, and whole-rock geochemistry. Major element analysis of olivine was conducted on the samples using a JEOL JXA-8230 Superprobe electron-probe microanalyzer (EPMA) at the University of Iowa equipped with five wavelength-dispersive spectrometers and large-format diffracting crystals. The beam conditions for olivine analysis were 20 keV accelerating voltage and a 200 nA beam current with the beam in spot mode. The EPMA was calibrated for Mg and Ni using San Carlos olivine (NMNH 111312-44) and Si, Fe, Ca, Ti, Mn, Cr, and Al using the Astimex Cr pyrope reference material. Calibrations for P used the Astimex apatite.

Peak positions for Ca, Al, Ti, Mn, Cr, and Ni were determined using long dwell times, 200 nA wavelength scans of San Carlos olivine (NMNH 111312-44; Jarosewich et al., 1980), and Kakanui augite (NMNH 122142; Jarosewich et al., 1987) and entered manually into the analytical routine before each analytical session. The peak position for P was updated using peak positions from the calibration standard. Major element peak positions were updated before analysis using software peak search routines. The total run-time per point was 7 minutes, with an on-peak dwell time of 40 seconds for major elements, 90 seconds for minor and trace elements except for Al, and a background dwell time of 15 total seconds for all elements except Al. Dwell times for Al were 360 seconds of on-peak and 60 seconds on background. Values obtained via EPMA for the San Carlos olivine were consistent with published values with variability (% r.s.d.; Jarosewich et al., 1980) of <1% for all elements, showing good consistency between the analytical runs. The detection limit for Al is 10 ppm and is between 20–30 ppm for other trace elements (Cr, Ni, P, Ca, and Ti). High-resolution backscatter electron (BSE) images of each crystal were taken to investigate crystal zonation and mark locations of electron microprobe analysis. Fifteen to twenty olivine phenocrysts from each sample were analyzed over three consecutive days. A minimum of two spots (core and rim) were analyzed in each olivine, with more detailed transects on 5–6 crystals from each sample. Two olivine phenocrysts from each thin section contain two transects along the elongated and short crystal axis. Transects were analyzed from core-to-rim where possible, using a 5-μm-step size. The selection of detailed transects was based on zonation observed in BSE images.

RESULTS

Olivine in the analyzed samples occurs as euhedral to anhedral phenocrysts, euhedral to subhedral phenocryst clusters (plus or minus clinopyroxene in glomerocrysts), and as groundmass crystal phases. Euhedral to subhedral olivine phenocrysts vary in size from 31–1200 μm in diameter. The largest crystals analyzed are from the distal northern OLP McCartys basalt (sample EMI-40-3). The smallest crystals are found nearest to the McCartys cone in the PLP group. Single euhedral crystals range in size from 90–1200 μm along the elongated axis with an average of 360 μm. Euhedral clusters of olivine in glomerocrysts range from 31–1015 μm with an average of 290 μm for single olivine and are generally smaller along the elongated axis than individual phenocrysts. All euhedral crystals contain rounded to elongated melt inclusions up to 42 μm in diameter. Skeletal or anhedral crystals are rare (only present in the southern sample EM142-2) and have melt inclusions that are more angular and smaller than in the euhedral crystals. Fe-Ti oxide and clinopyroxene reaction rims around olivine phenocrysts are absent in samples described in this study but are described by Kolsnik (1997) in samples from the TLP and PLP basalt groups. Chromite spinels are typical inclusions within the olivine phenocrysts. Melt embayments are present in some crystals as rounded intrusions filled with quenched glass. All melt embayments exhibit well-quenched glass with no evidence of co-entrapped phases or micro-phases. Some melt embayments terminate on polyhedral crystal faces; all exhibit evidence of matrix glass adjacent to the outlet bubble, indicating that the embayment was communicating with the surrounding melt. Rounded edges of embayment interiors suggest that they were formed through a slow-growth mechanism and are not remnants of healed crystal boundaries (Lloyd et al., 2014).

Compositional Zoning in Olivine

Major and trace element compositions of olivine phenocrysts are illustrated in Figures 2, 3, and 4, and representative analyses are presented in Table 1. McCartys Flow olivine ranges in forsterite contents (Fo#) from 91 to 32 and Mg-number (Mg#; Mg#=MgO/(MgO+FeO)*100) from 84 to 21. Ca (1770–3550 ppm, ±30 ppm) and P (0–1320 ppm, ±30 ppm) generally decrease with increasing Fo# (Fig. 2b, c), while Al (0–2170 ppm, ±10 ppm), and Ni (130–3220 ppm, ±30 ppm) generally increase (Figs. 2a, d, and 3). Ranges in Al and P contents are restricted in low Fo# olivine and show more variation for a given olivine composition at higher Fo# values (Fig. 2b, d).

Olivine phenocrysts generally have a thin rim/overgrowth (<40 um) of more Fe-rich olivine (Fig. 4a–d). Here a rim is defined as a compositional feature in contact with the glass, while a core is defined as the largest geochemically homogenous zone. The term mantle is used for all compositional zones

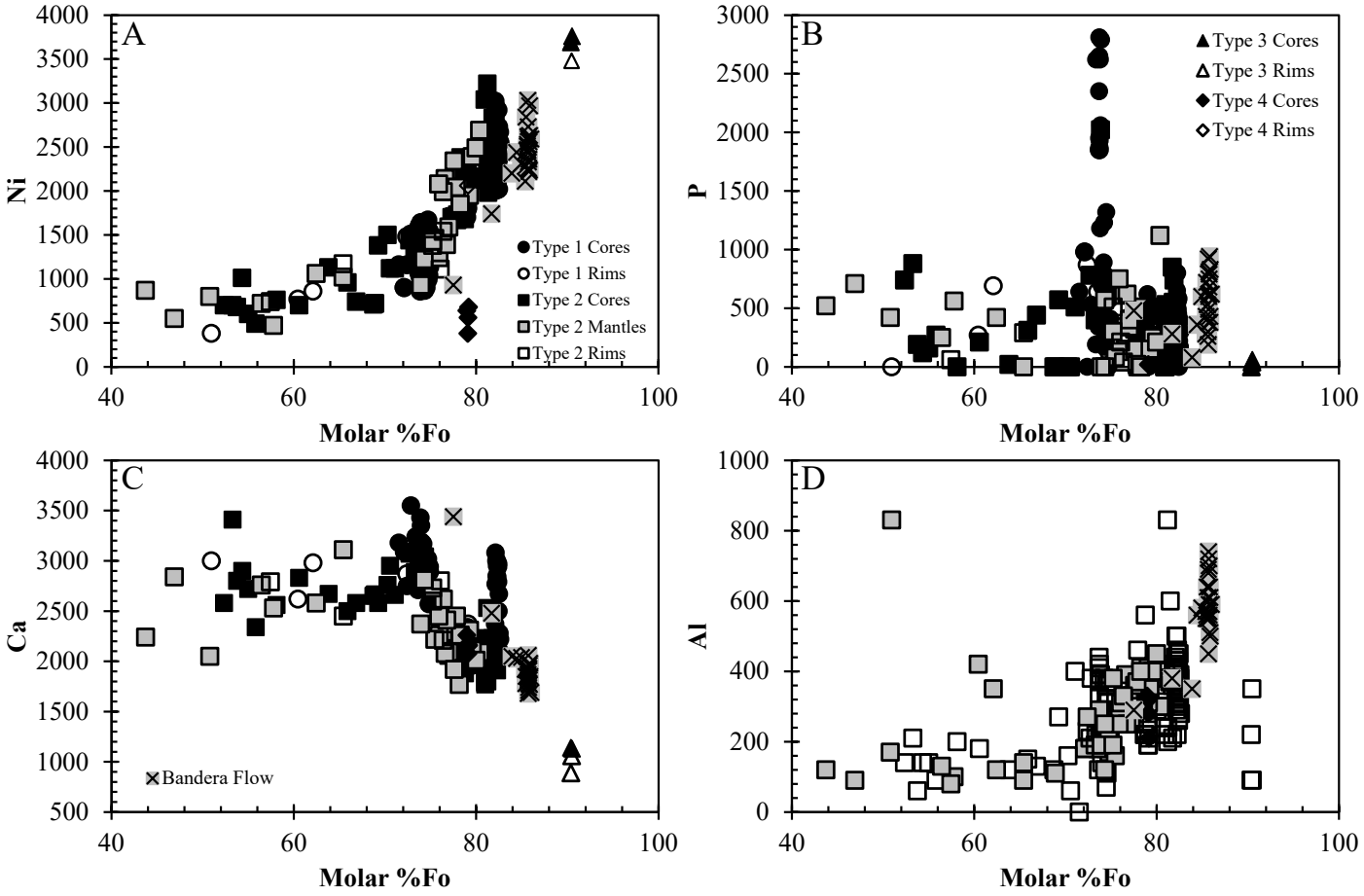

FIGURE 2. Variation diagrams for olivine phenocryst mineral chemistry from the McCartys and Bandera basalt flows. Trace elements are plotted against molar percent forsterite. McCartys Flow olivine are broken into crystal types described in text. Bandera Flow olivine phenocrysts are shown for reference and are homogeneous within a single crystal. Analytical uncertainties are equal to symbol size.

between the core and rim. Some olivine phenocrysts from the northern distal McCartys Flow samples show a more gradational normal Mg-Fe zoning profile followed by a thin high-Fe rim in contact with the glass. Four broad types of olivine are observed based on texture and core-to-rim major and minor element trends. Type 1 olivine phenocrysts are euhedral to subhedral (Fig. 4a, b), contain only cores and rims, and are the dominant (~65%) population of olivine phenocrysts analyzed. Core compositions range from $Fo_{72–86}$, have moderate Ca contents (1880–3550 ppm; Fig. 2c), and Ni contents between 870–3020 ppm (Figs. 2a, 3a). Rims are thin (<50 µm) with a lower Fo# ($Fo_{79–51}$) than cores of the same crystal. Olivine-hosted melt embayments are rare, but when present, are broad and rounded (Fig. 4a). Melt inclusions are present but are generally smaller than those observed in crystal types 2 and 3.

Type 2 crystals are the second most common type of olivine observed. Phenocrysts are euhedral to subhedral individual crystals or part of olivine and clinopyroxene glomerocrysts (Fig. 4d). These crystals contain cores ranging in Fo# from $Fo_{66–82}$, rims with $Fo_{31–82}$, and mantles from $Fo_{38–80}$ (Fig. 3b). For a given crystal, there is a general decrease in Ni (130–3220 ppm) and Cr (0–830 ppm) contents from core-to-rim and an increase in Ca (1770–3270 ppm) contents (Fig. 4c, d). Melt inclusions are the largest of the four crystal groups and melt embayments are rare. Type 3 crystals are euhedral isolated phenocrysts. Forsterite content is restricted from $Fo_{90–91}$ and is homogeneous within the core (Al=290–390 ppm, Ca=1130– to 1140 ppm, P=0–60 ppm, and Ni= 3690–3760 ppm, Figs. 2, 3c, and 4e). A ≤40µm rim is present on some type 3 olivine phenocrysts with $Fo_{87–88}$, which is generally 2–3% lower than the associated core (Fig. 4e). A few olivine phenocrysts from this crystal type have rims with an abrupt inversion of some compositional gradients near the crystal rim (i.e., hooked profiles), inferring a more complex diffusive process. Melt inclusions and embayments are rare in this group. Type 4 crystals are skeletal to anhedral phenocrysts and are rare. This population appears homogeneous ($Fo_{78–79}$, Al=210–330 ppm, Ca=2080–2260 ppm, P=410–510 ppm, and Ni= 1700–2340 ppm; Figs. 2 and 3d). No lower Fo# rim is observed in this phenocryst type. Melt inclusions are smaller, more abundant, and more elongate than those observed in other crystal types. Diffusive equilibration between the melt inclusions and the olivine is present in some olivine phenocrysts. Melt embayments are common with wide rounded entrances. All observed melt embayments in this olivine type have a well-quenched glass with no evidence of co-entrapped phases or micro-phases. Melt embayments terminate on polyhedral crystal faces, all exhibit evidence of matrix glass adjacent to the outlet bubble. We note there is some

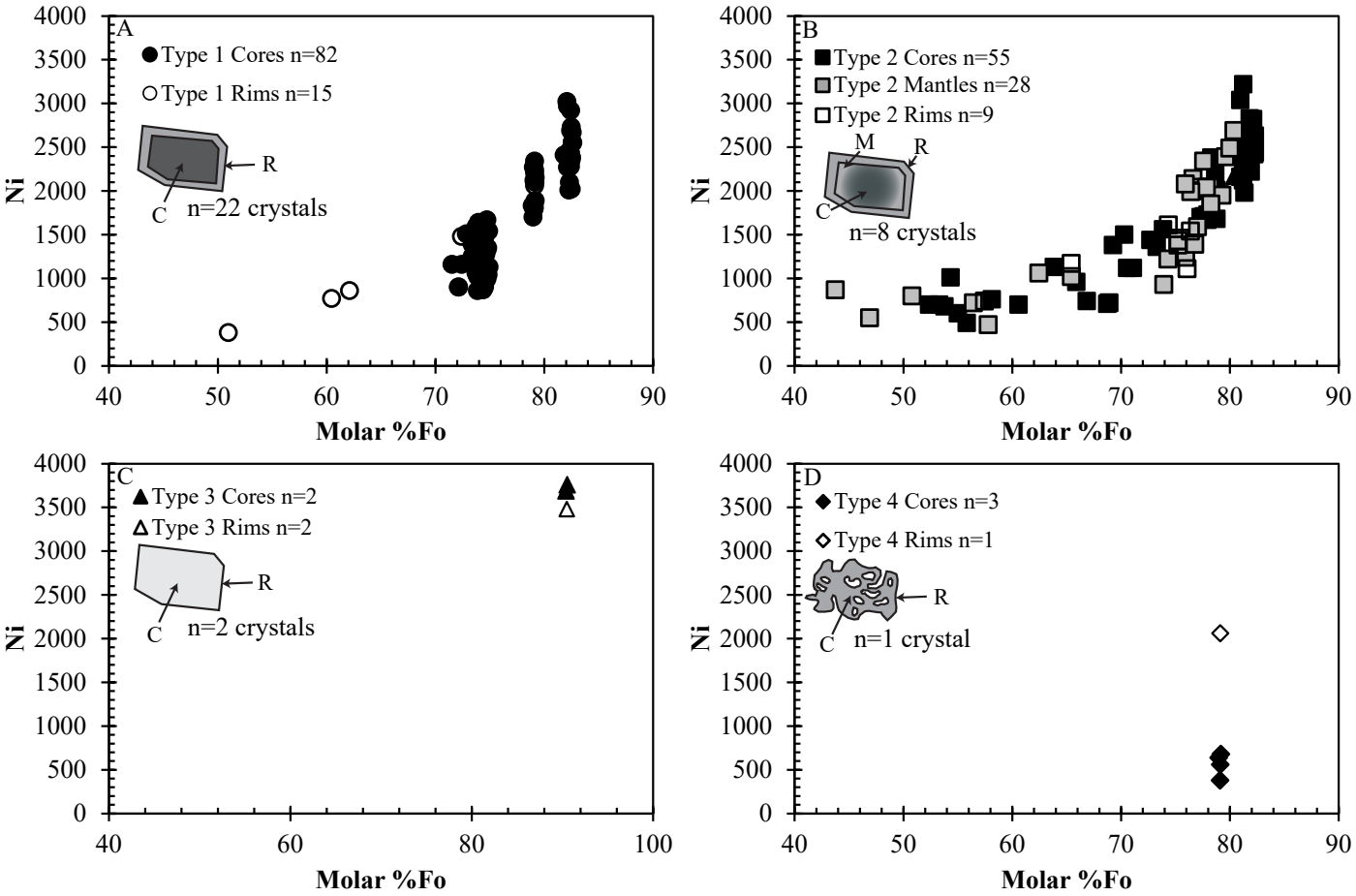

FIGURE 3. Nickel versus molar percent forsterite (Fo#) of McCartys Flow olivine phenocrysts. Analyses are divided by texture and by core, mantle, and rim analyses. **A**) Type 1 olivine are euhedral to subhedral crystals with homogeneous cores and lower Fo# and Ni-content rims. Core compositions fall into three general subgroups, $Fo_{70–75}$, $Fo_{78–79}$, and $Fo_{81–82}$. **B**) Type 2 olivine phenocrysts are euhedral to subhedral and contains core, mantle, and rims. Fo# and Ni contents decrease from core to rim for a single olivine phenocryst. Olivine phenocrysts from this group are found as individual crystals and in glomerocrysts with augite. **C**) Type 3 crystals are euhedral to subhedral crystals with homogeneous compositions. **D**) Type 4 olivine is anhedral with abundant olivine-hosted melt inclusions and melt embayments. Compositions are homogeneous for Fo# with rims containing higher Ni contents that the cores. Analytical uncertainties are equal to symbol size. C= core; M=mantle; R=rim.

variability in the abundances of olivine types in the samples from the northern distal samples and the southern sample. This is mainly evident in the lack of type 3 crystals in the northern distal sample (EMI-40-3) and type 4 phenocrysts only being observed in the southernmost extent of the flow (EM142-2).

DISCUSSION

Thermometry

Olivine-melt equilibrium provides insight into crystallization temperature, but more importantly, disequilibrium can be an indicator of olivine inheritance. We applied the water and pressure-sensitive olivine-liquid thermometer of Putirka (2008; eqns. 14 and 22), which provides an uncertainty of ±45°C. Water content estimates are not available for the McCartys Flow. We assume the melt is relatively anhydrous based on previous studies of other tholeiitic lavas in the Zuni-Bandera volcanic field and other intraplate basalts related to the Jemez lineament and Colorado Plateau (Peters et al., 2008; Reid et al., 2012; Rowe et al., 2015). Regardless of water content, a 2% variation would only change the calculated temperatures by 38°C, which is within the estimated uncertainty of Putirka (2008, eqns. 14 and 22). The pressure of olivine crystallization is uncertain, but geophysical models suggest the lithosphere-asthenosphere boundary beneath the Colorado Plateau is 65 km, and only 40 km at Mount Taylor just to the north of the ZBVF (Schmidt et al., 2016; Deng et al., 2017). We use an estimate of ~30–40 km translating to ~800–1000 MPa. We also note that a range in pressures from 400 MPa to 1000 MPa only changes the temperature estimate by 12°C, which is well within the calculated uncertainty of the equations (Putirka, 2008). Equilibrium versus disequilibrium was assessed using the method proposed by Roeder and Emslie (1970) and displayed on Rhodes diagrams (Rhodes et al., 1979). The test compares the observed Fe-Mg exchange coefficient with a constant value. Experimental data indicate a $KD_{(Fe-Mg)}$ value of 0.30±0.03 between olivine and liquid effectively determines olivine solubility for a given whole-rock Fe/Mg ratio. This value is independent of temperature, providing a method to determine if olivine coexists in equilib-

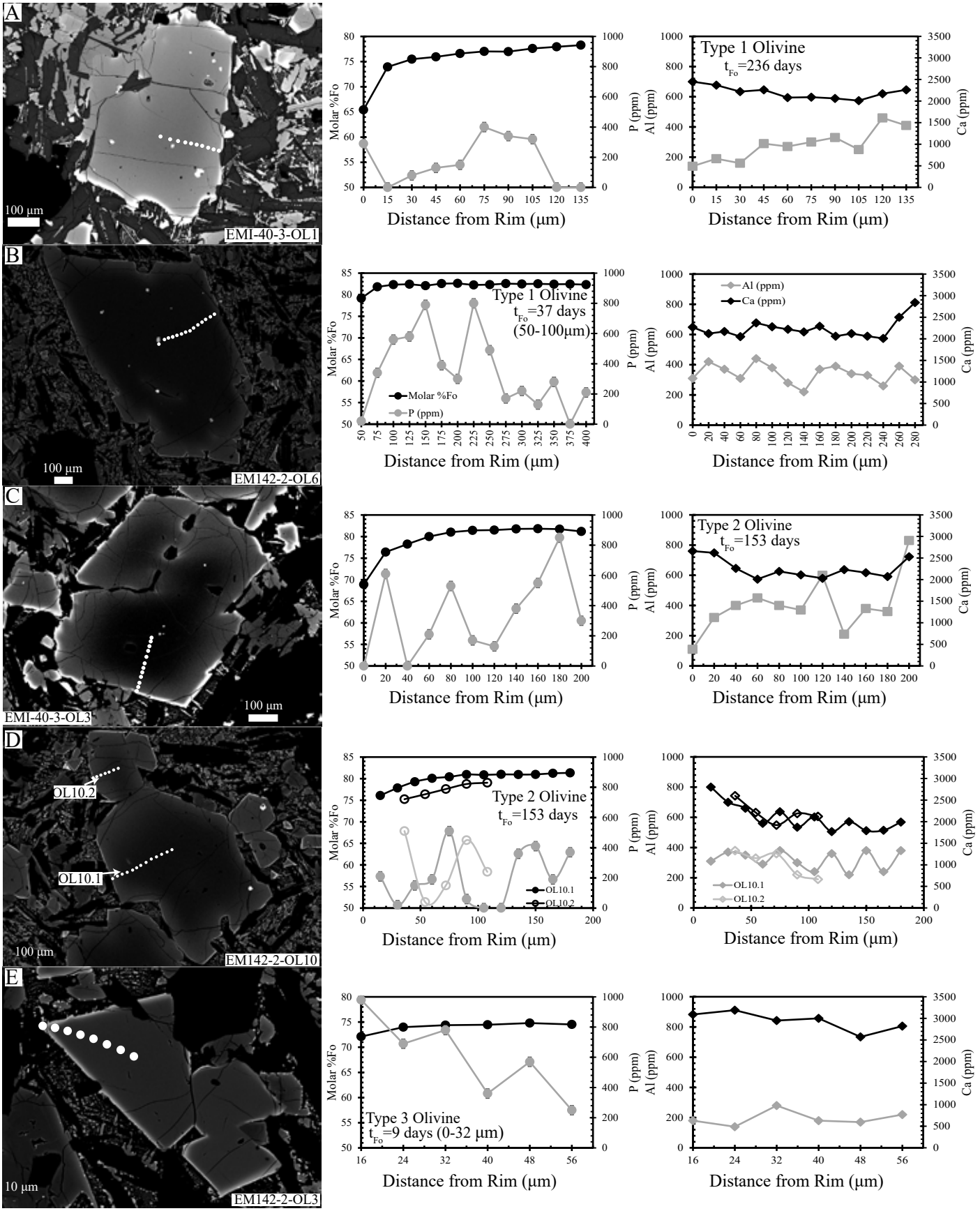
A
100 µm
EMI-40-3-OL1
Molar %Fo
P (ppm)
Al (ppm)
Ca (ppm)
Distance from Rim (µm)
Type 1 Olivine
t_{Fo}=236 days
B
100 µm
EM142-2-OL6
Type 1 Olivine
t_{Fo}=37 days
(50-100µm)
Molar %Fo
P (ppm)
Al (ppm)
Ca (ppm)
C
EMI-40-3-OL3
100 µm
Type 2 Olivine
t_{Fo}=153 days
D
OL10.2
OL10.1
100 µm
EM142-2-OL10
OL10.1
OL10.2
E
10 µm
EM142-2-OL3
Type 3 Olivine
t_{Fo}=9 days (0-32 µm)

TABLE 1. Olivine spot analyses (wt%), selected to show diversity in compositons.

	EMI-40-3OL1			EMI-40-3OL2			EM142-2OL1		EM142-2OL2		EM142-2OL3.1		EM142-2OL5.1	
Crystal Type	***Type 2***			***Type 2***			***Type 3***		***Type 3***		***Type 1***		***Type 1***	
Analysis Site	*core*	*mantle*	*rim*	*core*	*mantle*	*rim*	*core*	*rim*	*core*	*rim*	*core*	*rim*	*core*	*rim*
SiO_2	38.88	39.13	37.14	39.83	39.43	38.62	40.72	41.26	40.51	41.03	38.57	37.84	38.44	38.06
MgO	40.44	39.82	32.15	43.57	41.49	37.92	50.09	50.02	50.14	49.98	38.18	36.43	38.25	36.47
Al_2O_3	0.04	0.03	0.01	0.04	0.04	0.03	0.04	0.04	0.03	0.02	0.02	0.02	0.03	0.03
CaO	0.23	0.21	0.25	0.21	0.21	0.30	0.11	0.11	0.11	0.09	0.28	0.31	0.29	0.29
TiO_2	0.02	0.00	0.02	0.00	0.00	0.02	0.01	0.00	0.01	0.01	0.02	0.03	0.03	0.05
P_2O_5	n.d	0.04	0.03	0.03	0.03	n.d	0.01	0.00	n.d	n.d	0.03	0.10	0.07	0.09
FeO	20.02	21.16	30.27	16.76	18.98	23.32	9.36	9.40	9.52	9.47	23.25	25.09	23.05	24.78
MnO	0.25	0.26	0.37	0.23	0.24	0.25	0.17	0.14	0.07	0.14	0.33	0.36	0.32	0.32
NiO	0.19	0.16	0.12	0.24	0.24	0.16	0.38	0.35	0.37	0.37	0.15	0.09	0.13	0.15
Cr_2O_3	0.08	0.08	0.01	0.01	0.07	0.02	0.01	0.04	0.05	0.00	0.06	0.01	0.05	0.02
Total	100.15	100.88	100.36	100.93	100.72	100.65	100.89	101.35	100.80	101.10	100.88	100.28	100.66	100.25
Mg#	66.89	65.30	51.50	72.22	68.61	61.92	84.25	84.19	84.05	84.07	62.16	59.21	62.40	59.54
%Fo	78.26	77.03	65.43	82.24	79.57	74.34	90.51	90.46	90.38	90.39	74.53	72.12	74.73	72.39
%Fa	21.74	22.97	34.57	17.76	20.43	25.66	9.49	9.54	9.62	9.61	25.47	27.88	25.27	27.61

rium with a liquid or if the olivine was inherited/entrained and in disequilibrium (Roeder and Emslie, 1970). A Fe^{2+}/Fe^{3+} ratio of 0.8991 was used based on the corresponding FMQ buffer and a global compilation of similar basalt composition magmas from non-arc settings (Bezos and Humler, 2005).

The range in olivine crystallization temperatures for the McCarty Flow samples is within the calculated uncertainty of the olivine-liquid geothermometer of Putirka (2008). Type 1 and 3 olivine cores and rims and type 2 olivine core, mantle, and rim populations display internally consistent distributions for a given group. A population (>90% olivine analyzed) of cores from type 1 and 2 olivine phenocrysts are in equilibrium ($KD_{(Fe\text{-}Mg)}$ = 0.30±0.03; Roeder and Emslie, 1970; Putirka, 2008) with the whole rock and produce a temperature of 1247–1253°C. A second population of cores, and the mantles and rims from these groups produced higher temperatures >1260°C, and are considered in disequilibrium ($KD_{(Fe\text{-}Mg)} \neq$ 0.30±0.03; Roeder and Emslie, 1970; Putirka, 2008) with the whole rock, and therefore, calculated temperatures are considered with caution. Additional analysis of melt inclusion glass or an additional geothermometer is required to fully resolve these data with high confidence. All type 4 olivine phenocrysts are in disequilibrium with the melt, and calculated temperatures are unreliable. Based on a limited temperature range distribution, we suggest the olivine cores from type 1 and 2 crystals are in equilibrium with the whole rock (Fig. 5a, b). The crystal-poor nature of the lava and the percentage of euhedral olivine provides further evidence type 1 and 2 olivine phenocrysts crystallized early in the melt. One data point represents type 4 olivine and not statistically represented in the data set. Calculated temperatures and testing for equilibrium could not be evaluated for type 4 crystals due to high calculated uncertainties associated with the limited data points. Whole rock olivine-free calculated temperatures were calculated using equation 14 of Putirka (2008). These calculated temperatures range from 1222–1225°C and are lower than the olivine-glass temperatures.

Melt Compositions from Olivine

The olivine phenocrysts analyzed in this study can be classified as autocrysts, xenocrysts, or antecrysts by estimating the melt composition during crystal nucleation and growth from crystal-melt partition coefficients and their textural features. Here we define an autocryst as a mineral formed in equilibrium with the contemporary magma; antecrysts as crystals formed

FIGURE 4. Backscatter electron images (BSE) and compositional transects of olivine phenocrysts from the McCartys Flow OLP basalts exhibiting the range of textures found. **A**) Type 1 olivine phenocrysts have a broad high-Fo# core that is equilibrium with the host whole rock melt composition, and a thin lower-Fo rim. Type 1 olivine phenocrysts have calculated diffusion residence times of 220–250 days for four transects. **B**) Type 1A olivine with higher-Fo# core compared to higher-Fo# type 1 crystals. Diffusion timescales modeled only for the outer 100 µm of the phenocryst with a calculated age of just over one month. Interior of the crystal did not produce a viable diffusion residence time. **C** and **D**) Type 2 olivine phenocrysts are subhedral crystals with high-Fo cores in equilibrium with the whole rock, a thick mantle with lower-Fo and a very low-Fo content thin rim that is highly resorbed in some crystals. Three modeled diffusion profiles from the group produced consistent timescales of ~150±10 days. **E**) Type 3 olivine displays homogenous crystal interiors with a lower forsterite and higher CaO content rim. Type 3 crystals produced two diffusion residence times. Calculated ages for the rims are less than two weeks. Cores of the crystals produce calculated residence times of ~10 years. Rims are less than 40 µm. White circles represent EPMA analysis locations.

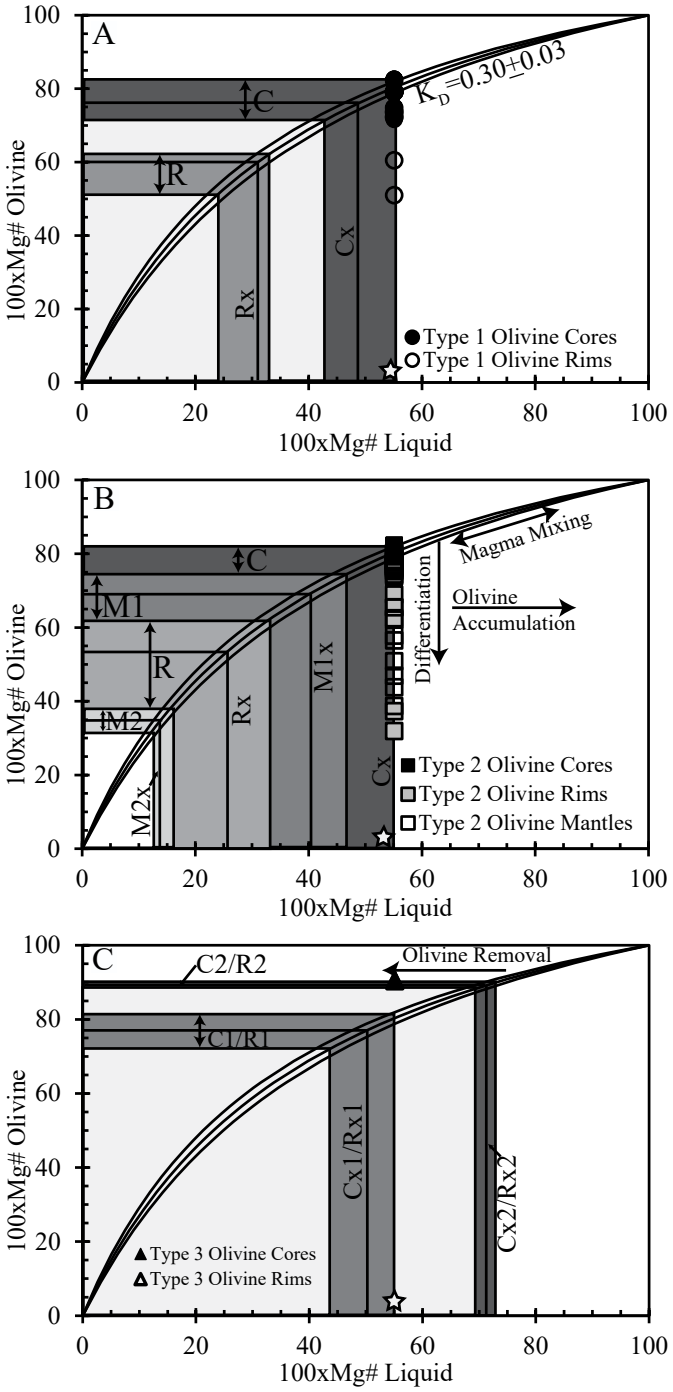

FIGURE 5. Mg#-olivine versus Mg#-liquid for olivine from the McCartys Flow. A-C) Inferred equilibrium-melt composition (Mg#) from measured olivine composition (Fo#), using Fe-Mg partition coefficients divided by olivine phenocryst type. Labeled arrows show schematically the effects of olivine accumulation and crystallization. Olivine cores from phenocryst types 1 and 2 are considered in equilibrium with the melt as represented by the whole-rock composition. Type 3 olivine phenocrysts are the result of olivine removal from a more primitive composition melt. Type 2 mantles and rims from olivine types 1, 2, and 3 are the result of olivine crystallization during melt differentiation. Rims, cores, and mantle data are separated and shown as the range in compositions found (arrows and grey shading). Means are marked by thick black lines inside the shaded area: Cx=mean core zone composition; Mx=mean mantle zone composition; and Rx= mean rim zone composition. Stars represent the whole rock composition.

in a previous magmatic episode; and xenocrysts as remnant minerals derived from their source or assimilated rock (Dungan and Davidson, 2004; Davidson et al., 2007; Coote et al., 2019; Przybylo et al., 2020). The groundmass in basalts in this study is mostly composed of micro-phenocrysts with minimal groundmass glass making the direct measurement of melt composition difficult. Using the whole-rock compositions and $KD_{(Fe\text{-}Mg)}$ criteria, most of the euhedral analyzed olivine cores from type 1 and 2 crystals. Some type 3 crystals are suggested to be in equilibrium with the whole rock (Fig. 5b). Rims from all olivine groups, type 2 mantles, and some type 4 core compositions are in disequilibrium (Fig. 5b, c).

The cores of type 1 phenocrysts ($Fo_{83–72}$, mean Fo_{77}) contain two populations of phenocrysts that re-equilibrated or nucleated in a melt (~Mg#=55) comparable to the host whole-rock composition (Fig. 5a). The first population ranges in Fo# from 72–75. The second has a slightly higher Fo# ranging from 79–83. On the criterion of their euhedral to subhedral shape and presence as individual crystals over glomerocrysts, they are considered autocrysts. Alternatively, these phenocrysts could have nucleated in a separate melt that coincidently was like the host rock, in which they would be antecrysts. However, these crystals are the dominant population of the olivine phenocrysts, consistent with an autocrystic origin. The type 1 olivine core compositions record the interior of the magmatic system sheltered from crustal contamination during magma ascent. The thin rim present in these olivine phenocrysts (as well as those observed in type 2 olivine) records the interaction with a more evolved melt (Mg#<55), likely during magma mixing, groundmass crystallization, or disequilibrium growth in response to rapid cooling. Further support includes the lack of melt embayments compared to type 2 and 4 olivine phenocrysts suggesting the olivine was in equilibrium during magma storage.

Equilibrium testing between type 2 crystal cores ($Fo_{66–82}$; mean Fo_{79}) and $Mg\#_{liquid}$ suggest multiple stability stages for these phenocrysts. Some type 2 phenocrysts with Fo# between 78–81 crystallized in a melt comparable to the whole rock (Mg#=55) and are autocrysts or re-equilibrated antecrysts. The remainder of the type 2 phenocrysts with Fo#<73 are in equilibrium with a melt with an Mg#<55 and record fractional crystallization/olivine crystallization during melt evolution. Mantle compositions of this olivine type are intermediate between the $Fo_{78–81}$ content cores and the lower forsterite content rims (Fig. 5b), suggesting the interaction of a more evolved melt (Mg#=55–25), potentially the same melt that crystallized the type 1 and 2 cores with $Fo_{<75}$. The compositional variation between the cores, mantles, and rims suggests these crystals either crystallized earlier during magma storage or experienced more evolved/contaminated melt compositions and cooler temperatures close to the exterior magma reservoir. This population of olivine is dominantly observed in glomerocrysts with clinopyroxene, suggesting inheritance into the melt during magma mixing over direct crystallization from the melt. The similar core Fo# to type 1 olivine suggests type 2 olivine cores crystallized in a melt like the host rock. If type 2 olivine were entrained/crystallized into the host magma during the main episode of olivine crystallization that produced the type

1 crystals, then the mantle compositions observed result from diffusion equilibration with a magma that is more evolved during magma differentiation. Lévesque and Ramos (2017) effectively modeled differentiation based on olivine-hosted melt inclusions and whole-rock compositions. These authors suggested that the isotopic and trace element signatures of the melt inclusions were consistent with crustal contamination and fractionation of olivine and plagioclase, producing a lower Mg# (<55) melt, which is suggested by the compositions of the olivine mantles and rims.

Type 3 homogeneous crystals ($Fo_{90–91}$) are nucleated in a melt with an Mg#>55 and are the result of olivine removal from a less evolved melt (Fig. 5c). These phenocrysts are considered either xenocrysts from partial melting of the mantle source or disaggregation of mantle xenoliths. An alternative is that these olivine phenocrysts are antecrysts inherited from the fractionated primary mantle melt. Based on the euhedral shape and lack of melt embayments or melt inclusions in these olivine phenocrysts, our preferred interpretation of inheritance from the parental melt. The "hooked" compositional profiles between the core and rims of the type 3 olivine could result from either a period of crystal overgrowth followed by diffusion or mixing of unzoned xenocrysts or antecrysts of olivine into compositionally different magma. To generate the hook profile, the new melt must not be in equilibrium with the overgrowth. Therefore, the crystal's chemical profile assumes an overgrowth that generates a low-Fo# plateau, followed by immersion of the crystal in a higher-Mg# melt, forming a new boundary condition and diffusivity, and creating the abrupt chemical gradient from core to rim. We assume that the diffusion inflection was caused by magma with a different chemical character than the host, creating a rim in disequilibrium. The compositional shift is likely associated with a magma mixing event between more primitive magma in equilibrium with type 3 cores recharging a storage system dominated by melt in equilibrium with type 1 and 2 olivine cores.

The anhedral/skeletal type 4 olivine phenocrysts with compositions of $Fo_{78–79}$ nucleated in a melt that was more evolved (Mg#<55) than the bulk rock composition. The initial anhedral textural appearance suggests these crystals could be skeletal, resulting from rapid crystal growth during magma ascent to the surface. We instead suggest that these olivine phenocrysts are highly resorbed after inheritance into the melt. Further support comes from P and Al contents in core-to-rim transects that do not show the fine-scale variation commonly documented in skeletal textures (Shea et al., 2019). The compositional variation observed in these crystals is more characteristic of diffusion equilibration; therefore, we consider this rare phenocryst type to be xenocrysts inherited/entrained during magma ascent from a more evolved basalt composition, likely from one of the older phases of volcanism in the Zuni-Bandera volcanic field.

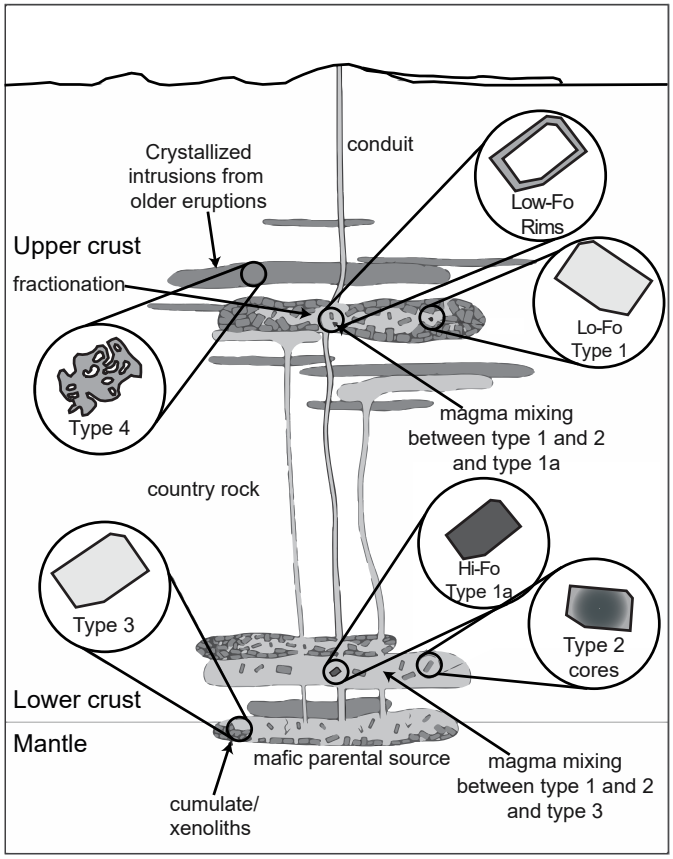

FIGURE 6. An integrated conceptual model of the basaltic magmatic conduit beneath the McCartys cinder cone explaining the textural and compositional characters of the olivine phenocrysts. The conceptual model is envisaged as a series of ephemeral conduits and chambers in space and time. Erupted basalts fractionate through a mafic parent in the lower crust or at the mantle-crust boundary accumulating or producing the Fo_{90} type 3 olivine. Type 1 (high-Fo#) and type 2 olivine cores ($Fo_{78–83}$) crystallize from the resulting basaltic melt in the lower crust. Type 2 olivine mantles are the result of further fractionation during magma ascent. During ascent, the basaltic magma encounters the crystallized remnants of previous plumbing systems which fed the older magmatic stages of the ZBVF and stalled crystal mush bodies in the mid to upper crust, entraining xenocryst type 4 olivine. Magma mixing between ascending magma with stalled magma mushes produce the $Fo_{<65}$ rims observed in type 1 and 2 olivine and new crystallization of euhedral $Fo_{<75}$ type 1 olivine phenocrysts. No lateral or vertical scale implied. Figure modified from Coote et al. (2019).

Implications for the ZBVF magmatic system

Variability in the olivine phenocryst core compositions suggests a vertically complex magmatic system for the monogenetic Zuni-Bandera volcanic field (Fig. 6), not unlike magmatic models proposed for polygenetic basaltic volcanoes, particularly for the Mount Taylor shield volcano to the north (Peters et al., 2008; Schmidt et al., 2016; Cashman et al., 2017). Unlike Mount Taylor, the ZBVF monogenetic clusters occur at isolated vents, and the ascending magma inferred from the McCartys Flow tholeiitic basalts can tap into an extensive array of stalled and solidified intrusions in the crust (Kolisnik, 1997; Peters et al., 2008; Levesque and Ramos, 2016; 2017; Schmidt et al., 2016; Goff et al., 2020).

The variability in the abundances of olivine types between the northern distal and southern samples (i.e., the lack of type 3 olivine in the northern distal sample) suggests variation in the plumbing system throughout the eruption. Type 3 olivine phenocrysts contain forsterite compositions like compositions

observed in the Bandera alkalic basalt (Fig. 2), suggesting some amount of source overlap (Laughlin et al., 1972; Levasque and Ramos, 2016). We suggest that the system is a series of ephemeral conduits and chambers in space and time with only short periods of magma storage at shallow depths (Fig. 6). This simple model integrates the magmatic systems and explains all the textures and compositional characters of the olivine assemblages.

Cognate olivine types 1, 2, and 3 cores provide insight into the deeper part of the magmatic system (>7 km depth; Kolsnik, 1997). Melt-crystal equilibrium and textures suggest these three crystal types represent autocrystic, antecrystic, and xenocrystic components. The most common olivine phenocrysts, type 1, nucleated in a melt compositionally equivalent to the host lava and are considered autocrystic, consistent with their euhedral to subhedral crystal shapes and the tendency for these crystals to be single isolated grains. These crystals contrast with type 3 olivine phenocrysts, which are in disequilibrium with the bulk rock, and crystallized in a melt that is more primitive than the host rock. These olivine phenocrysts are chemically similar to those observed in the Bandera Flow (Fig. 2), which is considered a primary mantle melt (Peters et al., 2008). Therefore, they are deemed antecrystic in origin and likely represent crystallization in the melt source, perhaps representing the episode of fractional crystallization that produced the fractionated melt as suggested by Levesque and Ramos (2016; 2017). Type 2 crystal cores are like the core compositions of the type 1a olivine. However, they are normally zoned from core-to-rim and show more significant variation in Fo#, Ni, and Ca contents than observed in Type 1 olivine and have euhedral crystal shapes, indicating prolonged residence in a more evolved melt. They are likely to be the product of mixing between cooling and fractionating magmas stalled in the shallow crust. Temperature estimates (T=1240–1260°C) for the mantles of type 2 olivine phenocrysts are within the clinopyroxene-melt equilibrium estimates of Kolisnik (1997; T= 1250–1300°C) at depths of 6–7 km. We suggest this is likely the location for interaction with magmas hosting the type 1 and type 4 olivine phenocrysts (Fig. 6). The highly resorbed type 4 crystals formed in a melt that was more evolved than that of the whole rock and, along with their texture, these data suggest type 4 olivine phenocrysts are xenocrystic in origin. Entrainment of these xenocrysts occurred during magma ascent from mafic intrusive forerunners that stalled and fractionated as they crystallized, likely from previous basaltic plumbing systems in the older episodes of volcanism in the ZBVF.

CONCLUSIONS

Preliminary analysis of olivine phenocrysts from the McCartys Flow suggests various compositions and textures divided into four distinct textural and compositional phenocryst types. Olivine types represent the differentiation and crystallization of mafic magma batches within a vertically extensive magmatic system. Large euhedral olivine phenocrysts with homogeneous compositions ($Fo_{78–82}$) are the most common. They nucleated in a melt equivalent to the host rock composition and are interpreted as autocrysts and record olivine fractionation from a parental mantle melt with magma residence times of about 5 months. Two subordinate euhedral to subhedral olivine types are present. The first type has core compositions like the type 1 crystals, but has normally zoned core-to-rim compositional profiles, suggesting fractionation and crystallization of the core, followed by either magma mixing or diffusion re-equilibration in a subvolcanic plumbing system. The second subordinate crystal type has Fo_{90} cores and records a sharp compositional inflection or "hook-shaped" diffusional profile recording a magma mixing event days before the eruption. This olivine type represents antecrysts from the parental melt.

Based on these olivine phenocryst crystal types, we suggest that the system is a series of ephemeral conduits in space and time with only short periods of magma storage at shallow depths. Homogeneous olivine core-to-rim transect compositions suggest residence times of one year or less, contrasting with the traditional view of rapid magma ascent from source to the eruption (McGee et al., 2012; 2013). If from the same source, three different zoned olivine populations must have been stored in magma bodies influenced by magma mixing to be able to develop different local chemical environments. Our results show that primitive magmas in small-volume monogenetic volcanoes have complex lithospheric magmatic histories and must have been stored in magma bodies influenced by an open system to develop different local chemical environments.

ACKNOWLEDGMENTS

Thoughtful and insightful reviews were provided by Brennan van Alderwerelt (Auburn University) and Jacob Siebach (Arkansas Tech), and editorial review by Fraser Goff, which greatly improved the manuscript. We also thank Bonnie Frey and Shari Kelley for editorial handling of this paper. This work was supported by internal funds from Missouri State University and an Affiliate Award from the NASA Missouri Space Grant Consortium to G. Michelfelder.

REFERENCES

Baldridge, W., Perry, F. V., Vaniman, D., Nealey, L., Leavy, B., Laughlin, A. W., Kyle, P., Bartov, Y., Steinitz, G., and Gladney, E., 1991, Middle to late Cenozoic magmatism of the southeastern Colorado Plateau and central Rio Grande rift (New Mexico and Arizona, USA): A model for continental rifting: Tectonophysics, v. 197, no. 2-4, p. 327-354. https://doi.org/10.1016/0040-1951(91)90049-X

Bézos, A., and Humler, E., 2005, The $Fe^{3+}/\Sigma Fe$ ratios of MORB glasses and their implications for mantle melting: Geochimica et Cosmochimica Acta, v. 69, no. 3, p. 711-725. https://doi.org/10.1016/j.gca.2004.07.026

Brenna, M., Cronin, S.J., Smith, I.E.M., Sohn, Y.K., Németh, K., 2010, Mechanisms driving polymagmatic activity at a monogenetic volcano, Udo, Jeju Island, South Korea: Contributions to Mineralogy and Petrology, v. 160, p. 931–950. https://doi.org/10.1007/s00410-010-0515-1

Carden, J.R. and Laughlin, A.W., 1974, Petrochemical variation within the McCartys basalt flow, Valencia County, New Mexico: Geological Society of America Bulletin, v. 85, p. 1479-1484. https://doi.org/10.1130/0016-7606(1974)85%3C1479:PVWTMB%3E2.0.CO;2

Cashman, K. V., Sparks, R. S. J., and Blundy, J. D., 2017, Vertically extensive and unstable magmatic systems: a unified view of igneous processes: Science, v. 355, no. 6331. https://doi.org/10.1126/science.aag3055

Coote, A., Shane, P., and Fu, B., 2019, Olivine phenocryst origins and mantle

magma sources for monogenetic basalt volcanoes in northern New Zealand from textural, geochemical and $\delta^{18}O$ isotope data: Lithos, v. 344-345, p. 232-246. https://doi.org/10.1016/j.lithos.2019.06.026

Costa, F., Dohmen, R. and Chakraborty, S., 2008, Time scales of magmatic processes from modeling the zoning patterns of crystals: Reviews in Mineralogy and Geochemistry, v. 69, no. 1, p. 545-594. https://doi.org/10.2138/rmg.2008.69.14

Costa, F., Shea, T., and Ubide, T., 2020, Diffusion chronometry and the timescales of magmatic processes: Nature Reviews Earth and Environment, v. 1, no. 4, p. 201-214. https://doi.org/10.1038/s43017-020-0038-x

Davidson, J.P.,Morgan, D.J., Charlier, B.L.A., Harlou, R., and Hora, J.M., 2007, Microsampling and isotopic analysis of igneous rocks: implications for the study of magmatic systems: Annual Reviews of Earth and Planetary Science, v. 35, p. 273–311. https://doi.org/10.1146/annurev.earth.35.031306.140211

Deng, F., Connor, C. B., Malservisi, R., Connor, L. J., White, J. T., Germa, A., and Wetmore, P. H., 2017, A geophysical model for the origin of volcano vent clusters in a Colorado Plateau volcanic field: Journal of Geophysical Research: Solid Earth, v. 122, no. 11, p. 8910-8924. https://doi.org/10.1002/2017JB014434

Dungan, M.A., and Davidson, J.P., 2004, Partial assimilative recycling of the mafic plutonic roots of arc volcanoes: an example from the Chilean Andes: Geology, v. 32, no. 9, p. 773–776. https://doi.org/10.1130/G20735.1

Dunbar, N. W., and Phillips, F. M., 2004, Cosmogenic ^{36}Cl ages of lava flows in the Zuni-Bandera volcanic field, north-central New Mexico, USA: Tectonics, geochronology, and volcanism in the Southern Rocky Mountains and Rio Grande rift: New Mexico Bureau of Mines and Mineral Resources Bulletin, v. 160, p. 51-59.

Goff, F., McIntosh, W., Peters, L., Wolff, J.A., Kelley, S.A., Goff, C.J., and Osburn, G.R., 2020, Volcanic evolution of Mount Taylor stratovolcano, New Mexico: Facts and misconceptions, *in* Frey, B., Kelley, S.A., Zeigler, K.E., McLemore, V.T., Goff, F., and Ulmer-Scholle, D.S. eds., Geology of the Mount Taylor Area: New Mexico Geological Society, Special Publication 14, p. 17-28.

Jarosewich, E.J., Nelen, J.A. and Norberg, J.A., 1980, Reference samples for electron microprobe analysis: Geostandards Newsletter, v. 4, p. 43–47. https://doi.org/10.1111/j.1751-908X.1980.tb00273.x

Jarosewich, E.J., Gooley, R. and Husler, J., 1987, Chromium augite — A new microprobe reference sample: Geostandards Newsletter, v. 11, p. 197-198. https://doi.org/10.1111/j.1751-908X.1987.tb00027.x

Johnson, E. R., and Cashman, K. V., 2020, Understanding the storage conditions and fluctuating eruption style of a young monogenetic volcano: Blue Lake crater (< 3 ka), High Cascades, Oregon: Journal of Volcanology and Geothermal Research, v. 408, p. 107103. https://doi.org/10.1016/j.jvolgeores.2020.107103

Kolisnik, A. M., 1997, Petrology of the McCartys lava flow sequence, Zuni-Bandera volcanic field, New Mexico [Ph.D. dissertation]: Calgary, University of Calgary, 337 p.

Laughlin, A., Brookins, D.G. and Causey, J.D., 1972, Late Cenozoic basalts from the Bandera lava field, Valencia County, New Mexico: Geological Society of America Bulletin, v. 83, p. 1543-1552. https://doi.org/10.1130/0016-7606(1972)83[1543:LCBFTB]2.0.CO;2

Laughlin, A., Perry, F., Damon, P., Shafiqullah, M., WoldeGabriel, G., McIntosh, W., Harrington, C., Wells, S., and Drake, P., 1993, Geochronology of Mount Taylor, Cebollita Mesa, and Zuni-Bandera volcanic fields, Cibola County, New Mexico: New Mexico Geology, v. 15, no. 4, p. 81-92.

Laughlin, A. W., Poths, J., Healey, H. A., Reneau, S., and WoldeGabriel, G., 1994, Dating of Quaternary basalts using the cosmogenic ^{3}He and ^{14}C methods with implications for excess ^{40}Ar: Geology, v. 22, no. 2, p. 135-138. https://doi.org/10.1130/0091-7613(1994)022%3C0135:DOQBUT%3E2.3.CO;2

Levesque, S.M., and Ramos, F.C., 2016, Geochemical variation of the McCartys Flow, west-central New Mexico: Evaluating the magmatic evolution of a continental tholeiitic basalt: Geological Society of America Abstracts with Programs, v. 48, no. 7. doi: 10.1130/abs/2016AM-286635

Levesque, S.M., and Ramos, F.C., 2017, Geochemical constraints on the magmatic evolution of the McCartys Flow, west-central New Mexico: Evaluating the magmatic evolution of a continental tholeiitic basalt: IAVCEI Program with Abstracts, p. 597.

Lloyd, A.S., Ruprecht, P., Hauri, E.H., Rose, W., Gonnerman, H.M., and Plan, T., 2014, NanoSIMS results from olivine-hosted melt embayments: Magma ascent rate during explosive basaltic eruptions: Journal of Volcanology and Geothermal Research, v. 283, p. 1-18. https://doi.org/10.1016/j.jvolgeores.2014.06.002

Magnani, M., Miller, K., Levander, A., and Karlstrom, K., 2004, The Yavapai-Mazatzal boundary: A long-lived tectonic element in the lithosphere of southwestern North America: Geological Society of America Bulletin, v. 116, no. 9-10, p. 1137-1142. https://doi.org/10.1130/B25414.1

McGee, L. E., and Smith, I. E. M., 2016, Interpreting chemical compositions of small scale basaltic systems: A review: Journal of Volcanology and Geothermal Research, v. 325, p. 45-60. https://doi.org/10.1016/j.jvolgeores.2016.06.007

McGee, L.E., Beir, C., Smith, I.E.M., Turner, S.P., 2011, Dynamics of melting beneath a small-scale basaltic system: a U-Th-Ra study from Rangitoto volcano, Auckland volcanic field, New Zealand: Contributions to Mineralogy and Petrology, v. 162, p. 547–563. https://doi.org/10.1007/s00410-011-0611-x

McGee, L. E., Millet, M.-A., Smith, I. E. M., Németh, K., and Lindsay, J. M., 2012, The inception and progression of melting in a monogenetic eruption: Motukorea Volcano, the Auckland volcanic field, New Zealand: Lithos, v. 155, p. 360-374. https://doi.org/10.1016/j.lithos.2012.09.012

McGee, L. E., Smith, I. E. M., Millet, M.-A., Handley, H. K., and Lindsay, J. M., 2013, Asthenospheric control of melting processes in a monogenetic basaltic system: A case study of the Auckland volcanic field, New Zealand: Journal of Petrology, v. 54, no. 10, p. 2125-2153. https://doi.org/10.1093/petrology/egt043

Menzies, M. A., Kyle, P. R., Jones, M., and Ingram, G., 1991, Enriched and depleted source components for tholeiitic and alkaline lavas from Zuni–Bandera, New Mexico: Inferences about intraplate processes and stratified lithosphere: Journal of Geophysical Research: Solid Earth, v. 96, no. B8, p. 13645-13671. https://doi.org/10.1029/91JB00556

Németh, K., Kereszturi, G., 2015, Monogenetic volcanism: personal views and discussion: International Journal of Earth Sciences (Geol. Rundsch.), p. 1-16. https://doi.org/10.1007/s00531-015-1243-6

Peters, T. J., Menzies, M., Thirlwall, M., and Kyle, P. R., 2008, Zuni–Bandera volcanism, Rio Grande, USA: Melt formation in garnet-and spinel-facies mantle straddling the asthenosphere-lithosphere boundary: Lithos, v. 102, no. 1-2, p. 295-315. https://doi.org/10.1016/j.lithos.2007.08.006

Przybylo, A., Pietranik, A., Schulz, B. and Breitkreuz, C., 2020, Towards identification of zircon populations in Permo-Carboniferous rhyolites of central Europe: Insight from automated SEM-mineral liberation analyses: Minerals, v. 10, no. 308. https://doi.org/10.3390/min10040308

Putirka, K. D., 2008, Thermometers and barometers for volcanic systems: Reviews in Mineralogy and Geochemistry, v. 69, no. 1, p. 61-120. https://doi.org/10.2138/rmg.2008.69.3

Re, G., Palin, J.M., White, J.D.L., and Parolari, M., 2017, Unravelling the magmatic system beneath a monogenetic volcanic complex (Jagged Rocks Complex, Hopi Buttes, AZ, USA): Contributions to Mineralogy and Petrology, v. 172, no. 94. https://doi.org/10.1007/s00410-017-1410-9

Reid, M.R., Bouchet, R.A., Blichert-Toft, J., Levander, A., Liu, K., Miller, M.S., and Ramos, F.C., 2012, Melting under the Colorado Plateau, USA: Geology, v. 40, no. 5, p. 387–390; https://doi.org/10.1130/G32619.1

Rhodes J.M., Dungan, M.A., Blanchard, D.P., and Long, P.E., 1979, Magma mixing at mid-ocean ridges: evidence form basalts drilled near 22°N on the mid-Atlantic ridge: Tectonophysics, v. 55, p. 35-61. https://doi.org/10.1016/0040-1951(79)90334-2

Roeder, P., and Emslie, R., 1970, Olivine-liquid equilibrium: Contributions to Mineralogy and Petrology, v. 29, no. 4, p. 275-289. https://doi.org/10.1007/BF00371276

Rowe, M. C., Lassiter, J. C., and Goff, K., 2015, Basalt volatile fluctuations during continental rifting: An example from the Rio Grande Rift, USA: Geochemistry, Geophysics, Geosystems, v. 16, no. 5, p. 1254-1273. https://doi.org/10.1002/2014GC005649

Rubin, A. E., Cooper, K. M., Till, C. B., Kent, A. J., Costa, F., Bose, M., Gravley, D., Deering, C., and Cole, J., 2017, Rapid cooling and cold storage in a silicic magma reservoir recorded in individual crystals: Science, v. 356, no. 6343, p. 1154-1156. https://doi.org/10.1126/science.aam8720

Schmidt, M. E., Schrader, C. M., Crumpler, L. S., Rowe, M. C., Wolff, J. A., and Boroughs, S. P., 2016, Megacrystic pyroxene basalts sample deep crustal gabbroic cumulates beneath the Mount Taylor volcanic field, New Mexico: Journal of Volcanology and Geothermal Research, v. 316, p.

1-11. https://doi.org/10.1016/j.jvolgeores.2016.02.020

Shea, T., Hammer, J.E., Hellebrand, E., Mourey, A.J., Costa, F., First, E.C., Lynn, K.J., and Melnik, O., 2019, Phosphorus and aluminum zoning in olivine: contrasting behavior of two nominally incompatible trace elements: Contributions to Mineralogy and Petrology, v. 174, no. 85. https://doi.org/10.1007/s00410-019-1618-y

Sims, K.W., Ackert Jr, R.P., Ramos, F.C., Sohn, R.A., Murrell, M.T., and DePaolo, D.J., 2007, Determining eruption ages and erosion rates of Quaternary basaltic volcanism from combined U-series disequilibria and cosmogenic exposure ages: Geology, v. 35, no. 5, p. 471-474. https://doi.org/10.1130/G23381A.1